Biochimica et Biophysica Acta 1838 (2014) 2870–2881

Contents lists available at ScienceDirect

Biochimica et Biophysica Acta

journal homepage: www.elsevier.com/locate/bbamem

The cooperative behaviour of antimicrobial peptides in model membranes

Jianping Wang [a], Manuela Mura [b,c,1], Yuhua Zhou [a], Marco Pinna [b,c,*,1], Andrei V. Zvelindovsky [b,c,1], Sarah R. Dennison [c], David A. Phoenix [c,2]

[a] UCLan Biomedical Technology Ltd (Shenzhen), Shenzhen Virtual University Park, Shenzhen 518057, PR China
[b] Computational Physics Group, University of Central Lancashire, Preston PR1 2HE, UK
[c] Institute for Nanotechnology and Bioengineering, University of Central Lancashire, Preston PR1 2HE, UK

ARTICLE INFO

Article history:
Received 28 March 2014
Received in revised form 27 June 2014
Accepted 1 July 2014
Available online 19 July 2014

Keywords:
Antimicrobial peptide
Membrane
Molecular dynamics
Cooperative effect
Secondary structure
Amino acid

ABSTRACT

A systematic analysis of the hypothesis of the antimicrobial peptides' (AMPs) cooperative action is performed by means of full atomistic molecular dynamics simulations accompanied by circular dichroism experiments. Several AMPs from the aurein family (2.5,2.6, 3.1), have a similar sequence in the first ten amino acids, are investigated in different environments including aqueous solution, trifluoroethanol (TFE), palmitoyloleoylphosphatidylethanolamine (POPE), and palmitoyloleoylphosphatidylglycerol (POPG) lipid bilayers. It is found that the cooperative effect is stronger in aqueous solution and weaker in TFE. Moreover, in the presence of membranes, the cooperative effect plays an important role in the peptide/lipid bilayer interaction. The action of AMPs is a competition of the hydrophobic interactions between the side chains of the peptides and the hydrophobic region of lipid molecules, as well as the intra peptide interaction. The aureins 2.5-COOH and 2.6-COOH form a hydrophobic aggregate to minimize the interaction between the hydrophobic group and the water. Once that the peptides reach the water/lipid interface the hydrophobic aggregate becomes smaller and the peptides start to penetrate into the membrane. In contrast, aurein 3.1-COOH forms only a transient aggregate which disintegrates once the peptides reached the membrane, and it shows no cooperativity in membrane penetration.

1. Introduction

Modern increase in antibiotic-resistance bacterial infections urges the development of new and non-conventional therapeutic agents with novel mechanisms of antimicrobial action [1,2]. Bioactive peptides, which are usually short molecules up to 50 amino acids, can be found in diverse range of organisms including plants, mammals, amphibians and insects. They are potential candidates to fulfil this role and some of the peptide antibiotics are currently in clinical trials [3–5].

How peptides with antimicrobial actions kill the bacteria is subject to continuous research [5–8]. Three different models for peptide-membrane interaction are commonly used: barrel-stave, toroidal and carpet models[9–11]. It was suggested that collective behaviour of peptides can play a role in the bacterial membrane destruction [12–19]. For instance, using ^{31}P oriented solid-state NMR experiments it was found that at high peptide concentration alamethicin adopts a transmembrane conformation while the novicidin forms a toroidal pore in the membrane [16]. Using solid-state ^{19}F NMR it was shown that at low concentration the amphiphilic $[KIGAKI]_3$ peptide binds to membrane as flexible β-strand, without forming any intra or intermolecular H-bonds [13]. At higher concentrations $[KIGAKI]_3$ self-assembles into immobilized β-sheets which lie flat on the membrane surface as amyloid-like fibrils. Combining fluorescence assay, SEM, and AFM characterisation Chen et al. [15] suggested a detergent-like mechanism of antimicrobial action where A_9K peptide self-assemble into the rod-like micelles, which pierce through the membrane leading to its lysis. In a recent experimental study a novel mechanism of peptide-induced cell lysis was proposed which is due to the peptide self-assembly into exosome-like aggregates [17]. Such self-assembly requires a strong collective behaviour of several antimicrobial peptides (AMPs).

Molecular dynamics (MD) simulations have been applied to understand the conformation and mechanism of AMPs, as well as related viral and cell-penetrating peptides [20,21]. MD simulation studies on the timescale of tens to hundreds of nanoseconds have successfully helped to model or refine the conformation of AMPs and their aggregation in the presence of membrane-mimicking solvent mixtures, detergent micelles, and lipid bilayers [22–32]. Several studies employed coarse-grained MD (CG-MD) to investigate the behaviour of peptide/

* Corresponding author.
E-mail address: mpinna.uclan@gmail.com (M. Pinna).
[1] Present address: Computational Physics Group, School of Mathematics and Physics, Brayford Pool, University of Lincoln, LN6 7TS.
[2] Present address: London South Bank University, 103 Borough Road, London SE1 0AA, UK.

http://dx.doi.org/10.1016/j.bbamem.2014.07.002
0005-2736/

complexes into lipid membrane [33–35] (see also an extensive review on CG-MD by Shinoda and collaborators) [36]. Using coarse-grained MD Sansom and co-workers found that the AMP maculatin 1.1. forms membrane-inserted aggregates, which allow for a water permeation through a fluctuating channel [34,37]. Using MD simulation Ref. [22] has shown that the peptide CM15 has a strong tendency to form α-helices inside in a ratio of 1:2 of palmitoyloleoylphosphatidylcholine (POPC) and palmitoyloleoylphosphatidylglycerol (POPG) membranes. Using MD Chen and Mark found that short peptides, aurein 1.2 and citropin 1.1, disrupt the membrane via a detergent-like mechanism inducing high local curvature while longer peptides such as maculatin 1.1 and the caerin 1.1 induce longer range curvature stabilizing the membrane pores [38]. Pourmousa et al. studied trasportan peptide in dipalmitoylphosphatidylcholine (DPPC) lipid bilayer finding that the lysine residue facilitates the process of diffusion of the peptide inside the membrane [27]. Investigating the behaviour of melittin in DPPC lipid bilayer Sengupta et al. found the formation of disordered toroidal pores at the high concentration of the peptide [19]. It has been shown that the charged residues of melittin play a crucial role in the pore formation in DPPC [19] and POPC [39]. Using the full atomistic MD in our previous work we found that the probability of penetration of AMP peptide aurein 2.3 inside the membrane is larger for higher AMP concentration [40]. However, a systematic study of the peptides' behaviour at higher concentrations with a full atomistic resolution in the presence of different environments is still lacking [7,41]. In this study we report combined MD and experimental results on single and multiple AMPs from aurein family. We have chosen a set of peptides with a broad range of antimicrobial activities (aurein 2.5-COOH, 2.6-COOH and 3.1-COOH). In order to investigate the influence of amino acid sequence on the cooperativity behaviour the choice was limited to the peptides, which have most of the sequences in common (starting ten amino acids). Moreover, the choice of aurein 3.1 was motivated by the presence of a polar histidine HIS residue instead of a hydrophobic amino acid (alanine or valine). The presence of histidine can change the peptide-membrane interaction and enhance or inhibit the peptide–peptide interaction. It was found that HIS-rich AMPs have a broad range of antimicrobial activity [42]. Therefore, their detailed investigation can help in designing new antimicrobial agents. In the present work the peptides were interacting with palmitoyloleoylphosphatidylethanolamine (POPE), and (POPG) lipid bilayers. The two membranes have different chemical properties: POPE is a zwitterionic lipid bilayer while POPG is an anionic lipid bilayer. POPE and POPG were chosen since they are the main components of Gram-positive bacteria, such as *Bacillus cereus*[43], some strains of which can cause severe foodborne diseases.

2. Materials and methods

2.1. Materials

Phospholipids 1-palmitoyl-2-oleoyl-sn-glycero-3-phosphoethanolamine (POPE) and 1-palmitoyl-2-oleoyl-sn-glycero-3-phosphoglycerol (POPG) were obtained from AVANTI polar lipid and used without further modification. The peptide analogues of aurein peptides: aurein 2.5-COOH (GLFDIVKKVVGAFGSL-COOH), aurein 2.6-COOH (GLFDIAKKVIGVIGSL-COOH) and aurein 3.1-COOH (GLFDIVKKIAGHIAGSI-COOH) were synthesized by SevernBiotech by solid state synthesis and purified by HPLC to purity greater than 95%. 2,2,2-Trifluoroethanol (TFE) and all other solvents and reagents were supplied by Fisher Scientific UK.

2.2. Circular dichroism measurements

Circular dichroism (CD) was recorded on a J-815 spectropolarimeter (JASCO, UK) equipped with a peltier temperature control unit using a 10 mm path-length cell over a wavelength range of 260 to 180 nm at a scan speed of 50 nm/min, 1 nm band width, and data pitch 0.5 nm. Far-UV CD spectra were collated for each peptide (0.01 mg/ml) in H_2O, PBS buffer (pH 7.4) and 100% TFE. CD experiments were also performed at a peptide:lipid ratio 1:100. To obtain small lamellar vesicles (SUVs), a predetermined amount of dried (5 mg/ml) POPG and POPE were dissolved in chloroform, evaporated under a stream of nitrogen, placed under vacuum overnight. The lipid film was then rehydrated using 1 × phosphate-buffered saline (PBS, pH 7.5) and sonicated 1 h or until the solution was no longer turbid. SUVs were then extruded 11 times through a 0.1 μm polycarbonate filter using an Avanti polar lipid mini-extruder apparatus. All CD experiments were obtained by acquiring 10 scans on a J-815 spectropolarimeter (Jasco, UK) and samples maintained at 30 °C. For all spectra acquired, the baseline acquired in the absence of peptide was subtracted. The percentage α-helical content was then estimated using CDSSTR algorithm (protein reference set 3) on the DichroWeb server [44–46]. These experiments were repeated four times and the percentage helicity was averaged.

2.3. Simulations

The mechanism of interaction between each aurein analogue and either 0.1 mol/l aqueous solution, TFE, POPE, and POPG was examined using molecular dynamics (MD). The aurein peptide analogues were each assembled as canonical α-helix using AMBER tools 1.4. Simulations and the analysis have been performed using GROMACS [47,48]. The simple point-charge (SPC) water model has been used [49]. The GROMOS 53a6 force fields for POPE and POPG was employed [50,51]. All structures have been equilibrated at room temperature in water in the following sequence: minimization, NVT and NPT simulation. In all cases the peptides have been positioned at 3 nm from the top leaflet of the lipid bilayer with his axis perpendicular to the interface of lipid bilayer and water [40]. The counter ions Na^+ and Cl^-have been added to neutralize the systems. All structures have been equilibrated at 303 K in the sequence minimisation: NVT and NPT simulations. A 200 ns equilibration at 303 K has been performed. An equilibration run of 2 ns has been carried out for the peptide–lipid bilayer system with the position of the peptide restrained using harmonic restraints with a force constant of 1.0 kJ^{-1} nm^{-2} per atom[38,51,52]. The cut off for both van der Waals and Coulombic interactions is 1.2 nm. Berendsen temperature coupling is used at 303 K while the water and the bilayer were coupled separately with coupling time of 0.1 ps for single groups. A semi-isotropic Berendsen barostat is used with coupling time of 2.0 ps [50,51]. The main molecular dynamic simulations (no restraints) have been performed at constant temperature, pressure and number of molecules. In order to calculate the angle between the lipid bilayer and the peptide the post-processing tool with GROMACS is used. The trajectories have been generated by extracting the coordinates every 20,000 steps. Bond lengths have been constrained using the LINCS algorithm [53]. The MD simulations have been performed in the NPT ensemble using periodic boundary conditions. The components for each system are shown in Table 1.

3. Results

3.1. Secondary structure of aureins in solutions and in presence of lipid bilayer

3.1.1. Experiments

Secondary structure analysis was performed using CD spectral data. Fig. 1A shows the solution structure of aurein 2.5-COOH, aurein 2.6-COOH and aurein 3.1-COOH. Far-UV CD spectra of the three peptides in PBS buffer and in water environment at neutral pH showed an unordered structure. However, in the presence of TFE, CD spectra (Fig. 1B) show two minima at 220 nm and 207 nm and a maximum at 195 nm for each of the peptides, which is characteristic of α-helical structure. The estimated helical content is 28% for aurein 2.5-COOH, 75% for aurein 26-COOH and 63% for aurein 3.1-COOH. The presence of POPE

Table 1
Details of the molecular dynamics simulations.

Water environment				
		Box size (nm)	Water	Ions
Single aurein	A 2.5	5.0 × 5.0 × 5.0	4059	$^{1}Cl^{-}$
	A 2.6	5.0 × 5.0 × 5.0	4042	$^{8}Na^{+}$:$^{9}Cl^{-}$
	A 3.1	5.0 × 5.0 × 5.0	4036	$^{8}Na^{+}$:$^{9}Cl^{-}$
Three aureins	A 2.5	8.0 × 8.0 × 8.0	16,856	$^{3}Cl^{-}$
	A 2.6	7.0 × 7.0 × 7.0	11,117	$^{21}Na^{+}$:$^{24}Cl^{-}$
	A 3.1	6.8 × 6.8 × 6.8	10,180	$^{19}Na^{+}$:$^{22}Cl^{-}$
TFE environment				
Single aurein	A 2.5	5.0 × 5.0 × 5.0	531	$^{1}Na^{+}$:$^{2}Cl^{-}$
	A 2.6	5.0 × 5.0 × 5.0	532	$^{1}Na^{+}$:$^{2}Cl^{-}$
	A 3.1	5.0 × 5.0 × 5.0	532	$^{1}Na^{+}$:$^{2}Cl^{-}$
Three aureins	A 2.5	7.7 × 6.8 × 6.8	1355	$^{11}Na^{+}$:$^{14}Cl^{-}$
	A 2.6	7.7 × 6.8 × 6.8	1390	$^{11}Na^{+}$:$^{14}Cl^{-}$
	A 3.1	7.7 × 6.8 × 6.8	1368	$^{11}Na^{+}$:$^{14}Cl^{-}$
POPE 128 lipids				
Single aurein	A 2.5	6.0 × 6.1 × 11.6	9034	$^{1}Cl^{-}$
	A 2.6	6.0 × 6.1 × 11.9	9036	$^{1}Cl^{-}$
	A 3.1	6.1 × 6.2 × 11.3	9038	$^{1}Cl^{-}$
Three aureins	A 2.5	6.0 × 6.1 × 11.3	8638	$^{3}Cl^{-}$
	A 2.6	6.0 × 6.1 × 11.6	8695	$^{3}Cl^{-}$
	A 3.1	6.1 × 6.2 × 11.2	8684	$^{3}Cl^{-}$
POPG 128 lipids				
Single aurein	A 2.5	6.8 × 6.8 × 9.9	9796	$^{128}Na^{+}$:$^{1}Cl^{-}$
	A 2.6	6.8 × 6.8 × 9.9	9805	$^{128}Na^{+}$:$^{1}Cl^{-}$
	A 3.1	6.8 × 6.8 × 10.0	9791	$^{128}Na^{+}$:$^{1}Cl^{-}$
Three aureins	A 2.5	6.8 × 6.8 × 9.9	9418	$^{128}Na^{+}$:$^{3}Cl^{-}$
	A 2.6	6.8 × 6.8 × 9.8	9476	$^{128}Na^{+}$:$^{3}Cl^{-}$
	A 3.1	6.7 × 6.7 × 10.0	9473	$^{128}Na^{+}$:$^{3}Cl^{-}$

liposomes induced helicity but at a lower level compared to the TFE data with 32.3% (aurein 2.5-COOH), 36.7% (aurein 2.6-COOH), and 38% (aurein 3.1-COOH) respectively (Fig. 1C). The presence of POPG (Fig. 1D) induced higher levels of helicity than POPE at 38% (aurein 2.5-COOH),42% (aurein 2.6-COOH) and 58% (aurein 3.1-COOH).

3.1.2. MD simulations

Fig. 2 shows the secondary structure for aurein-COOH peptides in the presence of water and TFE as a function of time. The analysis of the secondary structure has been done according to Refs. [54,55]. The average of the single aurein and triple aurein helicity has been calculated over the last 50 ns of simulation. For aurein 2.5-COOH in water only residues 2–10 are α-helical (blue) up to 10 ns. After 10 ns there is a loss in helicity leading to other motifs such as bend, turn and coils and after 100 ns 50% of the aurein 2.5-COOH residues form three β-strands, which involve LEU2–PHE3, LYS8–VAL10, and PHE13–SER15. For aurein 2.6-COOH in water the initial α-helical structure was lost within 60 ns and the structure was predominantly β-sheet but included other motifs such as bends. After 200 ns, 38% of aurein 2.6-COOH residues form β-strand involving LEU2–VAL9, ILE10–ILE13, LYS8–SER15, the side chain of ASP4 and the backbone of LYS7. For aurein 3.1-COOH the peptide is a completely random coil after 200 ns (Fig. 3 and Table 2) in the presence of water. Fig. 3 shows that in a TFE environment, each of the aurein peptide analogues has a stable α-helix structure. The most stable configuration was observed for aurein 2.6-COOH (81%) while aurein 2.5-COOH, and aurein 3.1-COOH showed only 27% and 45% of α-helical structure respectively (Fig. 2 and Table 2). After 200 ns aureins GLY1–VAL10 in aurein 2.5-COOH maintained the initial stable α-helical configuration while the remaining residues become predominantly random coil. For aurein 2.6-COOH, after 200 ns the α-helical structure was

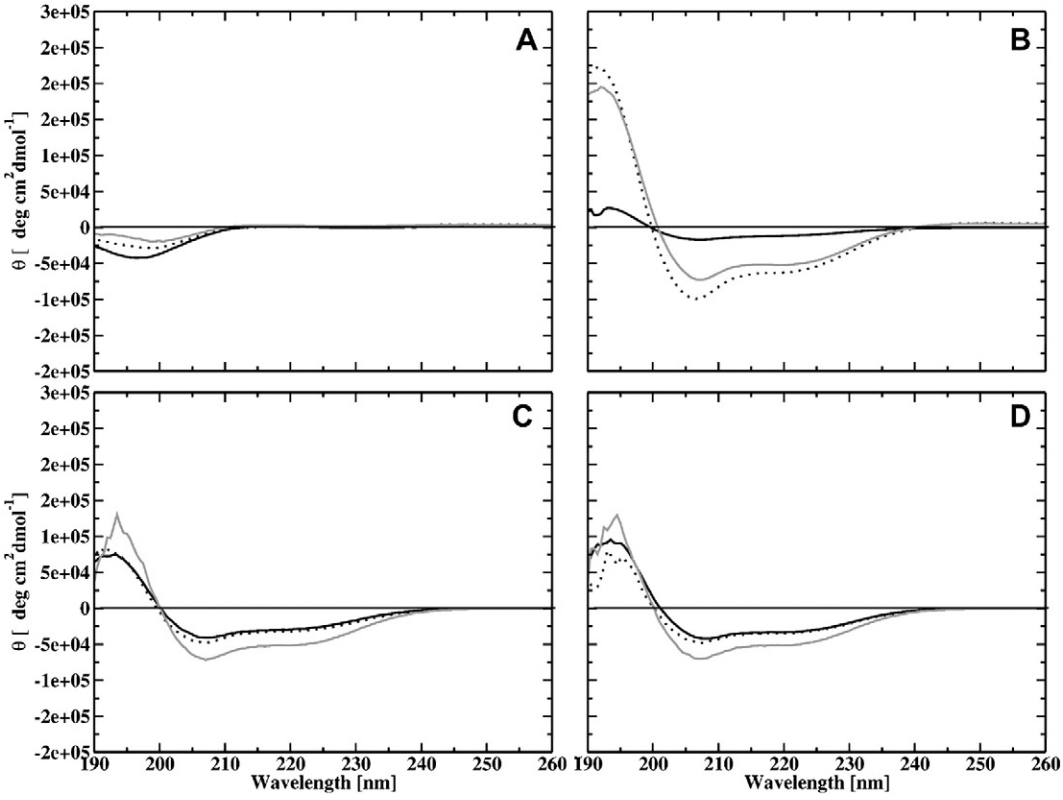

Fig. 1. CD spectra of aurein 2.5-COOH (black), aurein 2.6-COOH (dotted black) and aurein 3.1-COOH (grey) in the presence of aqueous solution (A), TFE (B), POPE (C) and POPG (D).

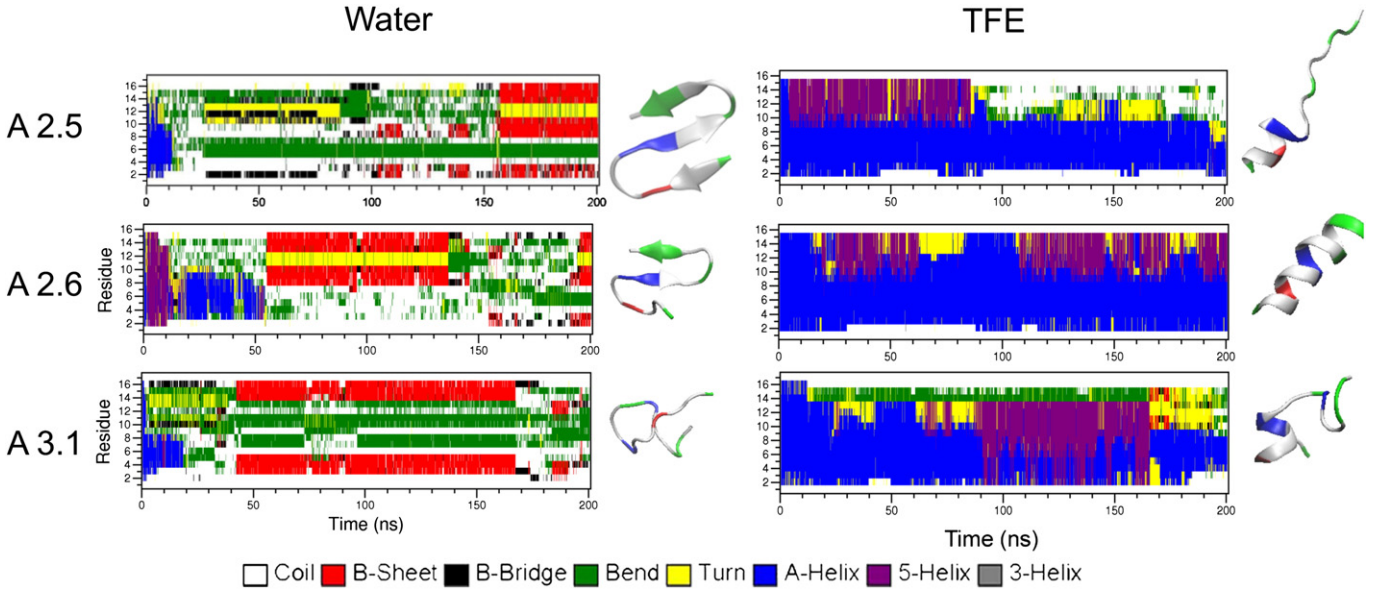

Fig. 2. The evolution of the secondary structure of single aureins 2.5, 2.6 and 3.1 in water and TFE.

maintained between residues GLY1 and GLY14 and for aurein 3.1-COOH only residues PHE3–ILE9 were predominantly α-helical.

3.1.3. Three peptides in solution

MD simulations containing three peptides were conducted in order to investigate the role of cooperativity in structure stabilisation. Fig. 3 shows the secondary structure profiles for three aurein-COOH peptides in the presence of water and TFE as a function of time. For aurein 2.5-COOH in the presence of water, after 200 ns, 38% of the residues of peptide A and 63% of residues of peptide B forms β-strands, while the peptide C is unstructured (Table 2). Peptide A has two intramolecular hydrogen bonds between LYS8–SER15 and VAL10–PHE13 and peptide B has two intramolecular hydrogen bonds formed between ASP4–GLY11 and VAL6–VAL9. The three peptides forms three intermolecular hydrogen bonds: ALA12–PHE13, GLY14–PHE13, and GLY14–SER15, respectively. Furthermore, LYS7 and LYS8 for each of the aurein 2.5-COOH peptide molecules protect the hydrophobic side chains from the access of water (Fig. 3 and Table 2). In contrast to aurein 2.5-COOH, the aurein 2.6-COOH peptide molecules in the presence of water exhibits a more stable α-helix and β-sheet. For the duration of the MD simulation peptides A and B remain helical between PHE3–VAL9 and ILE5–VAL12 respectively (38% and 25% helical see Table 2). Furthermore, for peptide A, after 180 ns residues ILE10–VAL12 and for peptide B, after 60 ns residues GLY14–SER15 are predominantly β-strands (25 and 31%; Table 2). In contrast to the other two peptides, peptide C displays an unfolded structure between 40 and 60 ns, however, after 60 ns the peptide displays 25% β-sheet configuration between VAL12–LEU16 (Table 2). The stabilisation of β-sheet is due to the hydrophobic interactions between the side chains of ILE, LEU, VAL, and PHE. In the case of aurein 3.1-COOH the three peptides aggregate together using their LEU2 and PHE3 residues. After 100 ns, for each of the three peptide molecules there is a loss of α-helix structure. For peptide A, after 200 ns, the peptide maintains a random coil structure whereas 24% of peptide B forms an unstable helical configuration (Table 2). Peptide C forms three β-strands with 35% of its residues but the two stable β-strands are positioned between peptides A and B, which are stabilized by hydrogen bonds between PHE3–ASP4 and GLY11–HIS12, while the third β-strand (GLY15–SER16) remains unstable for the duration of the simulation (Fig. 6 and Table 2). Fig. 3 shows that in a TFE environment, each of the aurein 2.5-COOH peptide molecules have a stable α-helix structure, which do not interact with each other at the start of the simulation. After 200 ns, aurein 2.5-COOH peptide A exhibits an α-helical configuration (37%; Table 2) which involved GLY1–ILE5 residues, however, peptide B also remained helical (44%; Table 2) involving LEU2–LYS8 while peptide C maintained a random coil configuration after 80 ns. For each aurein 2.6-COOH peptide the molecules maintained an α-helical configuration for the duration of the simulation. Aurein 2.6-COOH peptide A was 38% helical, which involved residues PHE3–LYS8, however, peptide B exhibited the highest percentage helicity (88%; Table 2) compared to the remaining peptide molecules. Here, LEU2–GLY14 residues maintain the α-helical in peptide B molecule whereas for peptide C is 38% α-helical and LEU2–VAL6 are responsible for maintaining this structure. For aurein 3.1-COOH, peptides A and B maintain an α-helical structure configuration for the duration of the simulation (38 and 25% respectively; Table 2) which involved the VAL6–ALA10 (peptide A) and LEU2–VAL6 (peptide B) residues. For aurein 3.1-COOH peptide C lost its helical configuration after 100 ns and a random coil structure is formed until 180 ns. After 180 ns, peptide C refolds to form an α-helical structure involving LEU2–VAL6.

3.1.4. Peptides in the presence of lipid bilayers

Figs. 4 and 5 show the secondary structures of single and triple aureins in POPG and POPE. In the presence of POPE aurein 2.5-COOH residues 2–10 are helical up to 20 ns, however, after that the peptide becomes predominately β-sheet (38%; Table 2) between residues LYS8–VAL10 and PHE13–LEU16. For aurein 2.6-COOH a stable helical (38% Table 2) structure between residues PHE3–VAL9 was maintained during the duration of the simulation. For aurein 3.1-COOH in presence of POPE the helical structure is initially unstable (50 ns) but after 150 ns a stablehelical conformation (41%; Table 2) emerges till the end of the simulation involving residues LEU2–LYS8. In contrast, to the case of POPE, in the presence of POPG each of the peptides was predominantly β-sheet. After 10 ns, 25% of aurein 2.5-COOH residues form a β-sheet structure, which involves GLY1–PHE3 and LEU5–LYS7. For aurein 2.6, after 5 ns the helix was destroyed and the peptide maintained a random coil configuration. In the case of aurein 3.1the helix was also destroyed after 10 ns and β-sheet configuration was maintained between VAL6–LYS8 and SER15–ILE16 for the duration of the simulation. For three aureins 2.5-COOH in the presence of POPE peptide A lost its α-helical configuration after 10 ns where a random coil structure was maintained for the duration of the simulation. However, aurein 2.5-COOH peptide B and C showed a stable α-helical configuration (31 and 38% respectively; Table 2) involving residues ILE5–VAL9 and PHE3–VAL9 respectively. A similar trend was observed for aurein 2.6-COOH peptide, where peptide

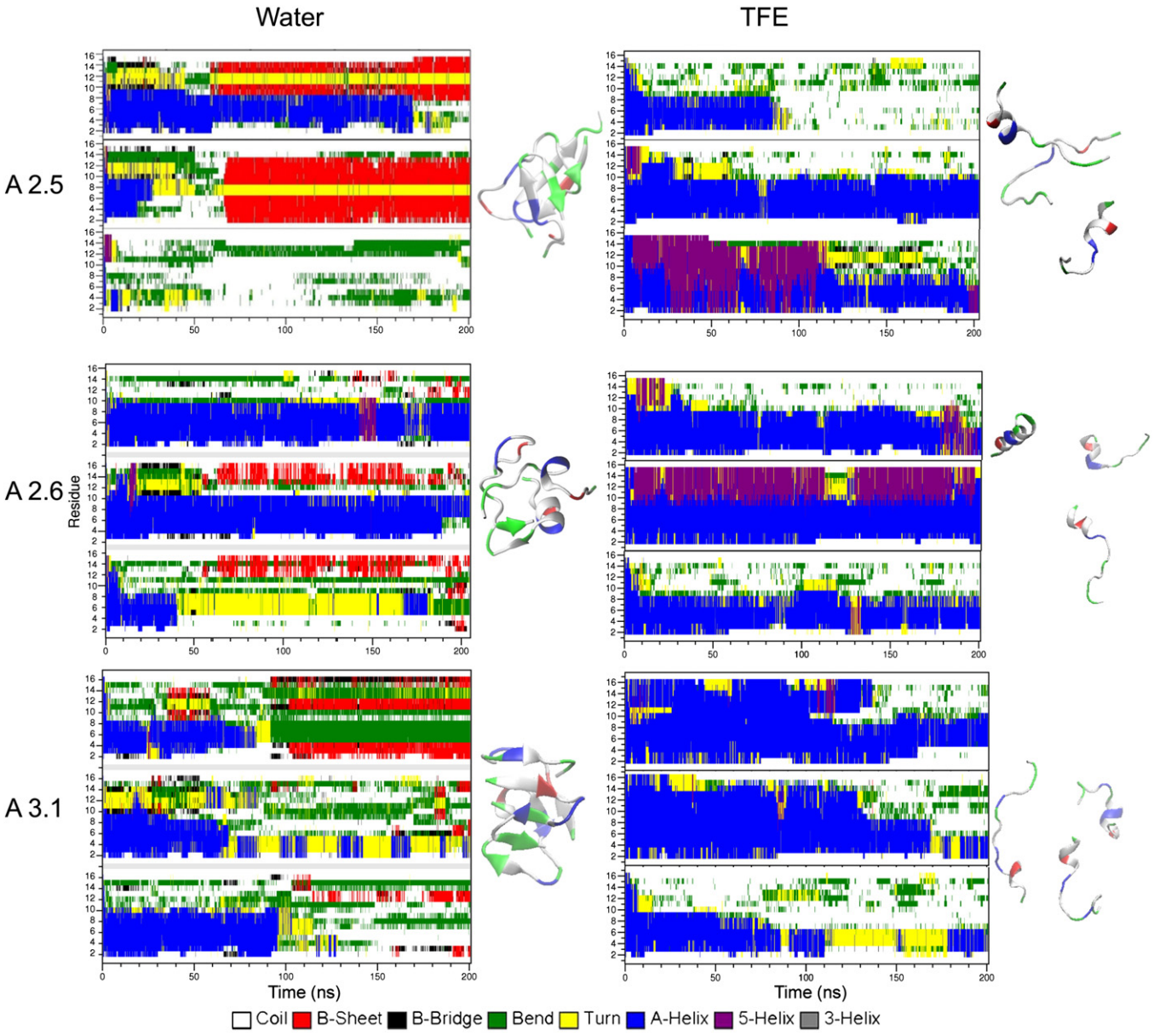

Fig. 3. The evolution of the secondary structure of three molecules of aurein 2.5, 2.6 and 3.1 in aqueous solution and TFE.

A loses its α-helical configuration after 40 ns. However, for aurein 2.6-COOH peptides B and C showed a stable α-helical configuration (56 and 44% respectively; Table 2) involving residues LEU2–GLY11 and PHE3–VAL9 respectively. In contrast to aurein 2.5-COOH and aurein 2.6-COOH, aurein 3.1-COOH was predominantly a random coil after 30 ns for each of the peptide molecules, which was maintained for the duration of the simulation. In the presence of POPG, each of the aurein peptide molecules behaved in a different manner compared to the case of POPE. Aurein 2.5-COOH peptide molecules maintain an α-helical configuration although for each peptide the stability varies. Aurein 2.5-COOH peptide A has a stable α-helical structure (38%; Table 2) involving ILE5–VAL9 although after 200 ns the amino acid residues involved in the stabilisation of the helix are LEU2–VAL9. Peptide B and peptide C maintained α-helical configuration (44 and 38%; Table 2) involving in both cases PHE3–VAL9. For aurein 2.6-COOH peptide A maintains an α-helical configuration (38%; Table 2) involving PHE3–ALA6, however, during the simulation the peptide structure fluctuates involving hydrogen bonds between PHE3 and VAL9. In contrast to aurein 2.6-COOH peptide A, peptide B and peptide C maintain stable α-helical structures (50% in both cases; Table 2) involving LEU2–VAL9 for both peptides. A similar trend to aurein 2.6-COOH is observed for aurein 3.1-COOH where peptide A showed an α-helical configuration (29%; Table 2) involving LEU2–ILE5, peptide B maintains47% in a stable α-helical configuration involving LEU2–HIS12. However, for aurein 3.1-COOH peptide C a higher percentage of helicity was observed (82%; Table 2) and the residues LEU2–ALA14 maintained the structure for the duration of the simulation. For aurein 2.5-COOH in the presence of POPE peptide A lost its α-helical configuration after 10 ns where a random coil structure was maintained for the duration of the simulation (Fig. 5). However, aurein 2.5-COOH peptide B and C showed a stable α-helical configuration (31 and 38% respectively; Table 2) involving residues ILE5–VAL9 and PHE3–VAL9 respectively. A similar trend was observed for aurein 2.6-COOH peptide molecules where peptide A lost its α-helical configuration after 40 ns (Fig. 5). Again for aurein 2.6-COOH peptides B and C showed a stable α-helical configuration (56 and 44% respectively; Table 2) involving residues LEU2–GLY11 and PHE3–VAL9 respectively. In contrast to aurein 2.5-COOH and aurein 2.6-COOH, aurein 3.1-COOH was predominantly random coil after 30 ns for each of the peptide molecules, which was maintained for the duration of the simulation (Fig. 5).

Table 2
The secondary structure of the aureins in different environments at 200 ns. Blue boxes: ratio of α-helix; Red boxes: ratio of β-sheet; the dash represents 100% random coil. The data are shown for single and three peptides (A, B and C letters denote each of the three peptides). The helicity for the single aurein as well for the three aureins has been averaged over the last 50 ns of the simulations.

				Water	TFE	POPE	POPG
Aurein 2.5	MD	Single		38 ± 15%	27 ± 17%	36 ± 6%	23 ± 8%
		Three	A	38%	37%	–	38%
			B	63%	44%	31%	44%
			C	–	–	38%	38%
		Average		42 ± 6%	27 ± 3%	22 ± 2%	37 ± 4%
		CD		–	28 ± 2%	32.3 ± 0.6%	38.0 ± 0.7%
Aurein 2.6	MD	Single		8 ± 16%	81 ± 10%	34 ± 6%	–
		Three	A	38% 25%	38%	–	38%
			B	25% 31%	88%	56%	50%
			C	60%	38%	50%	50%
		Average		29 ± 5% 9 ± 7%	50 ± 5%	31 ± 3%	41 ± 4%
		CD		–	75 ± 2%	36.7 ± 0.6%	42 ± 0.3%
Aurein 3.1	MD	Single		15 ± 16%	45 ± 17%	35 ± 7%	21 ± 11%
		Three	A	–	38%	–	29%
			B	24%	25%	–	47%
			C	35%	25%	–	82%
		Average		2 ± 3% 15 ± 7%	22 ± 7%	–	47 ± 4%
		CD		–	63 ± 2%	38 ± 2%	58 ± 3%

In the presence of POPG, each of the aurein peptide molecules behaved in a different manner compared to the case of POPE. Aurein 2.5-COOH peptide molecules maintain α-helical configurations although for each peptide the stability varies. Aurein 2.5-COOH peptide A has a stable α-helical structure (38%; Table 2) involving ILE5–VAL9 although after 200 ns the amino acid residues extended to LEU2–VAL9. Furthermore, peptide B and peptide C maintained α-helical configuration (44 and 38%; Table 2) involving in both cases PHE3–VAL9. For aurein 2.6-COOH peptide A maintains an α-helical configuration (38%; Table 2) involving PHE3–ALA6, however, during the simulation the peptide structure fluctuates involving hydrogen bonds between PHE3 and VAL9. In contrast to aurein 2.6-COOH peptide A, both peptide B and peptide C maintain a stable α-helical structure (50% in both cases; Table 2) involving LEU2–VAL9 for both peptides. A similar trend to aurein 2.6-COOH is observed for aurein 3.1-COOH where peptide A showed an α-helical configuration (29%; Table 2) involving LEU2–ILE5, peptide B maintains a stable α-helical configuration (47%) involving LEU2–HIS12. However, for aurein 3.1-COOH peptide C a higher percentage of helicity was observed (82%; Table 2) and here residues LEU2–ALA14 maintained the structure for the duration of the simulation.

3.2. Dynamics of peptides in the presence of a lipid bilayer

3.2.1. Single aurein in POPE

Fig. 6 shows MD simulation snapshots highlighting the interaction between the different aurein peptides and a POPE bilayer. The depth of penetration by each peptide is illustrated by the distance between the centre of mass of the peptide and top of PO_4 groups in POPE bilayer. After 20 ns aurein 2.6-COOH and aurein 3.1-COOH approaches the headgroups of the lipid bilayer whereas aurein 2.5-COOH remains in the water environment. After 70 ns each the aurein peptides lie parallel to the membrane surface.

In the case of POPE and aurein 2.5-COOH the peptide unfolds after 24 ns and the PHE3 residue forms a hydrogen bond with PO_4 groups in the bilayer whereas the C-terminus forms a β-strand due to hydrogen bonds between VAL10 and PHE13 andalso between LYS8 and LEU16. It takes 70 ns for the residues LEU2 and PHE3 to reach the membrane interface and form a hydrogen bond between the side chain of SER15 and the PO_4 group (Fig. 6). After 200 ns, the side chains of residues LEU2, PHE3, VAL10 and PHE13 orientate themselves towards the hydrophobic region of the lipid bilayer. The peptide then penetrates deep into the inner core region of the lipid bilayer (Fig. 6). However, in the case of aurein 2.6-COOH at the start of the simulation in the presence of a POPE bilayer, LEU2 and PHE3 orientates towards the lipid bilayer so that the water interacts with the alkyl chains of lipid molecules. After 200 ns, a hydrogen bond is formed between the carboxyl group of LEU16 and the PO_4 group of POPE bilayer. In addition, the side chains of hydrophobic residues LEU2, PHE3, ILE5, and LEU16 orientate towards the water/lipid interface (Fig. 6). For aurein 3.1-COOH in the presence of POPE, at the start of the simulation up to 20 ns HIS12 approaches the headgroups of the lipid bilayer. After 70 ns the peptide lies parallel to the membrane surface forming hydrogen bonds with the POPE headgroup region. At 200 ns the stable α-helical conformation orientates in such way that the HIS12 residue is attaching to the headgroups of POPE bilayer. The side chains of PHE3 and ILE17 form a hydrophobic region above the headgroups of the lipid bilayer (Fig. 6).

3.2.2. Multiple aureins in POPE

At the start of the simulation aurein 2.5-COOH peptides form a trimer (Fig. 6). The trimer is stabilized via the PHE residues interacting

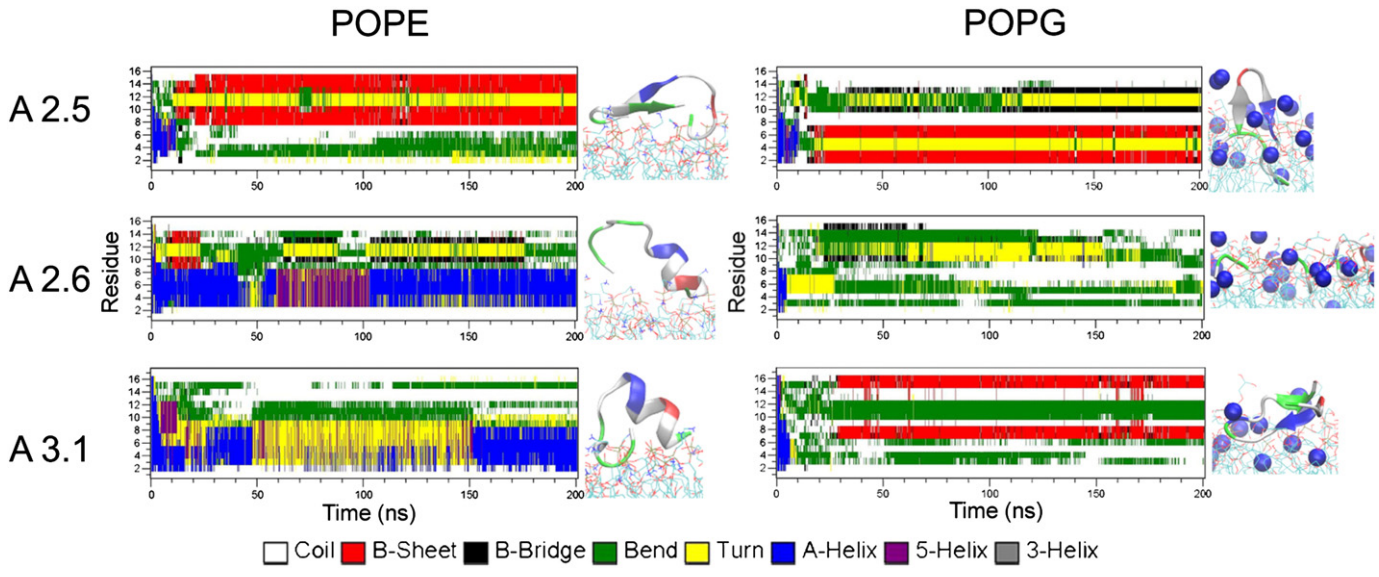

Fig. 4. The evolution of the secondary structure of single aureins 2.5, 2.6 and 3.1 in POPE and POPG.

with the hydrophobic residues LEU and VAL. First hydrogen bonds between the backbones of GLY14 and LEU16 of B peptide and the PO_4 groups of the lipid bilayer are formed. After 70 ns a partial penetration of the peptides into the headgroup region is observed. At the end of the simulation (200 ns), the trimer is more stable forming a hydrophobic pore with the PHE residues which surround the LEU and VAL. Hydrogen bonding is also observed in peptide B between SER15 and LEU16 and the PO_4 as well as the ammonium groups of lipids (Fig. 6). A similar behaviour is observed for aurein 2.6-COOH in the presence of the lipid bilayer (Fig. 6). Here, a pore is formed after 20 ns between the LEU2, PHE3, ILE10, ILE13, and LEU16 of peptides B while peptide C is capped by the side chain of LEU16 of peptide A. In addition, the backbone of GLY14 of peptide A and VAL9 of peptide C form a hydrogen bond. After 70 ns, there is an interaction between the hydrophobic pore and the head group of POPE which involves a hydrogen bond between GLY7 and PO_4 lipid bilayer. At the end of the simulation (200 ns) a stable pore is formed where the backbone of LEU2 of the peptide A forms a hydrogen bond with the PO_4 group of the lipid bilayer. Moreover, the side chains of the hydrophobic residues LEU2 and PHE3 are orientated towards the lipid headgroups. Here, the backbone of VAL12, GLY14, and SER15 residues of peptide B form three hydrogen bonds with the ammonium groups of lipid bilayer. The side chain of VAL12 penetrates deeper into the hydrophobic core region whereas the backbone of PHE3 forms a hydrogen bond with the PO_4 group of lipid bilayer. This in turn forces the amino group of GLY1 and the side chain of LEU2 of peptide C to insert deeper into the hydrophobic core region (Fig. 6). In contrast to aurein 2.5-COOH and aurein 2.6-COOH, aurein 3.1-COOH peptide monomers interact via hydrophobic interactions with the lipid bilayer. After 70 ns, the three peptides aggregate forming an unstable pore, which leads to peptide A and peptide B lying parallel to the membrane surface. However, after 200 ns peptide A GLY15 residue forms hydrogen bonds with peptide B ALA14 and GLY11 residues whereas the backbone of HIS12 in peptide B and GLY15 of peptide C forms hydrogen bonds with the PO_4 lipid bilayer. As a result this enables the three peptides to interact with the lipid membrane hence penetrate into the bilayer (Fig. 6).

3.2.3. Single aurein in POPG

Fig. 7 shows the interaction between the different aurein peptides and a bilayer formed by POPG. After 20 ns aurein 2.5-COOH and aurein 2.6-COOH interact with the headgroups of the lipid bilayer whereas aurein 3.1-COOH remains in the water environment. After 70 ns each of the peptides starts to penetrate into the membrane. In the case of aurein 2.5-COOH at the start of the simulation the peptide interacts

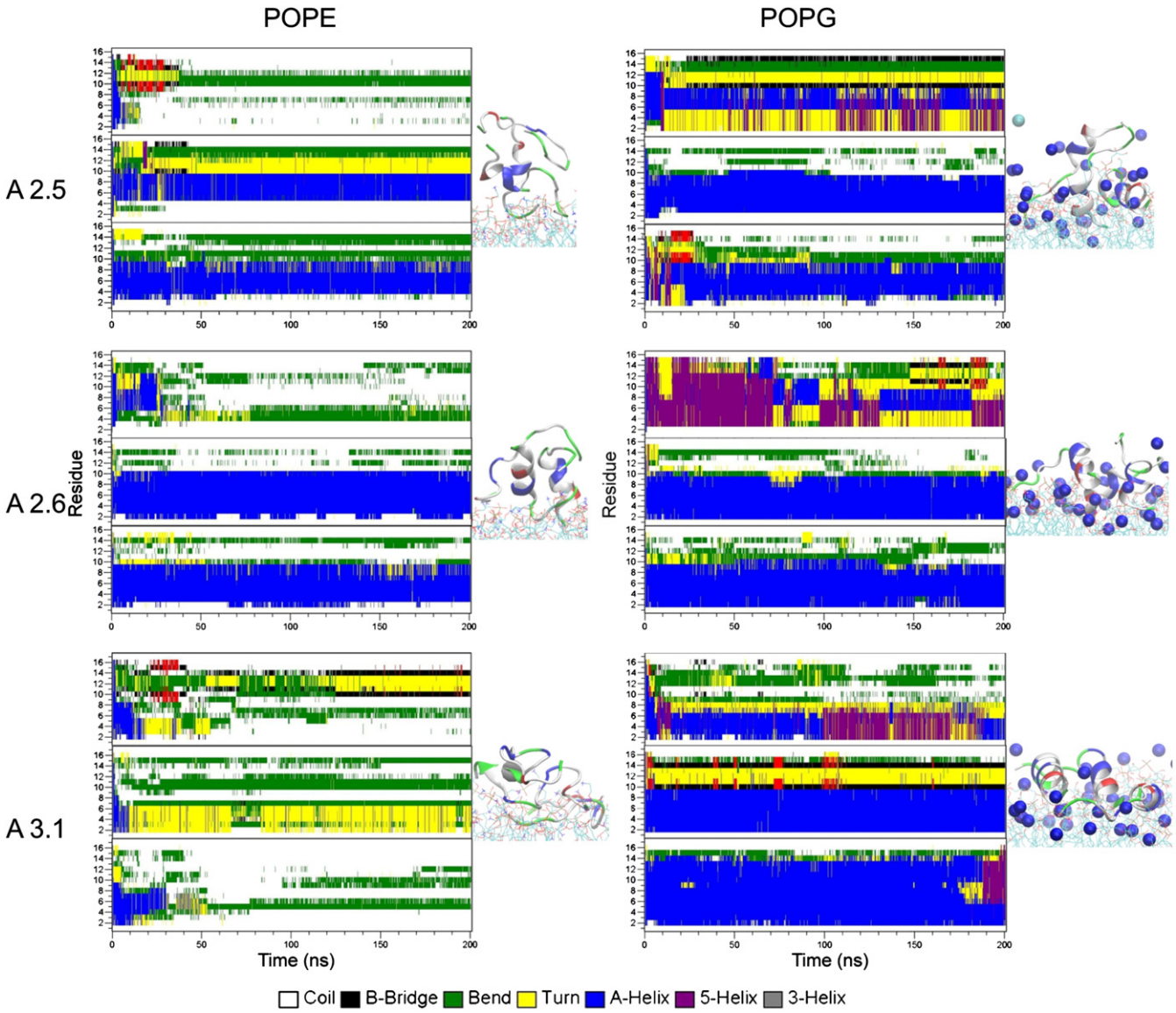

Fig. 5. The evolution of secondary structure of three molecules of aureins 2.5, 2.6 and 3.1 in POPE and POPG.

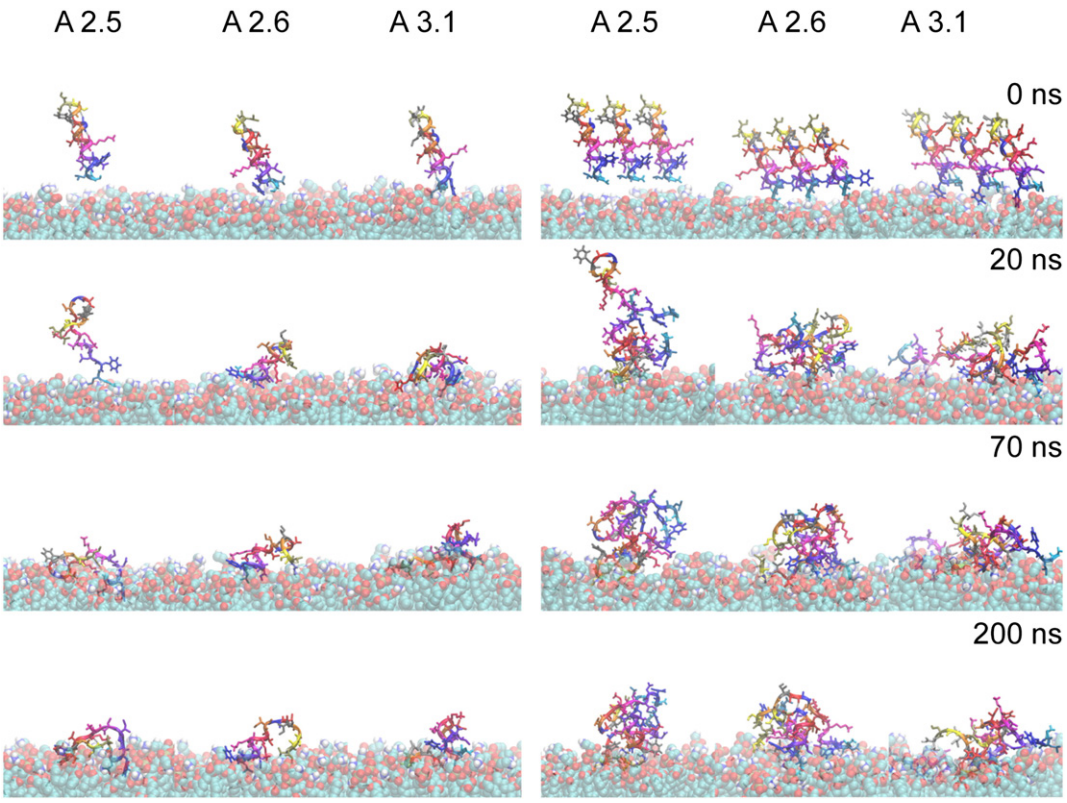

Fig. 6. Simulation snapshots of single and triple aureins with POPE lipid bilayers (times are indicated above the snapshots).

with the lipid headgroup of the lipid bilayer. After 70 ns the side chains of PHE13 and LEU16 interact with the hydrophobic core. The backbone of GLY14 and LEU16 forms two hydrogen bonds with PO_4 group. After 200 ns PHE3 inserts into the membrane and the side chains of VAL10, PHE13 and LEU16 penetrate into the hydrophobic core region. In contrast to aurein 2.5-COOH, at the start of the simulation the aurein 2.6-COOH interacts with the headgroup region of the lipid bilayer. After 70 ns residues LYS9–LEU16 orientate perpendicular to the membrane

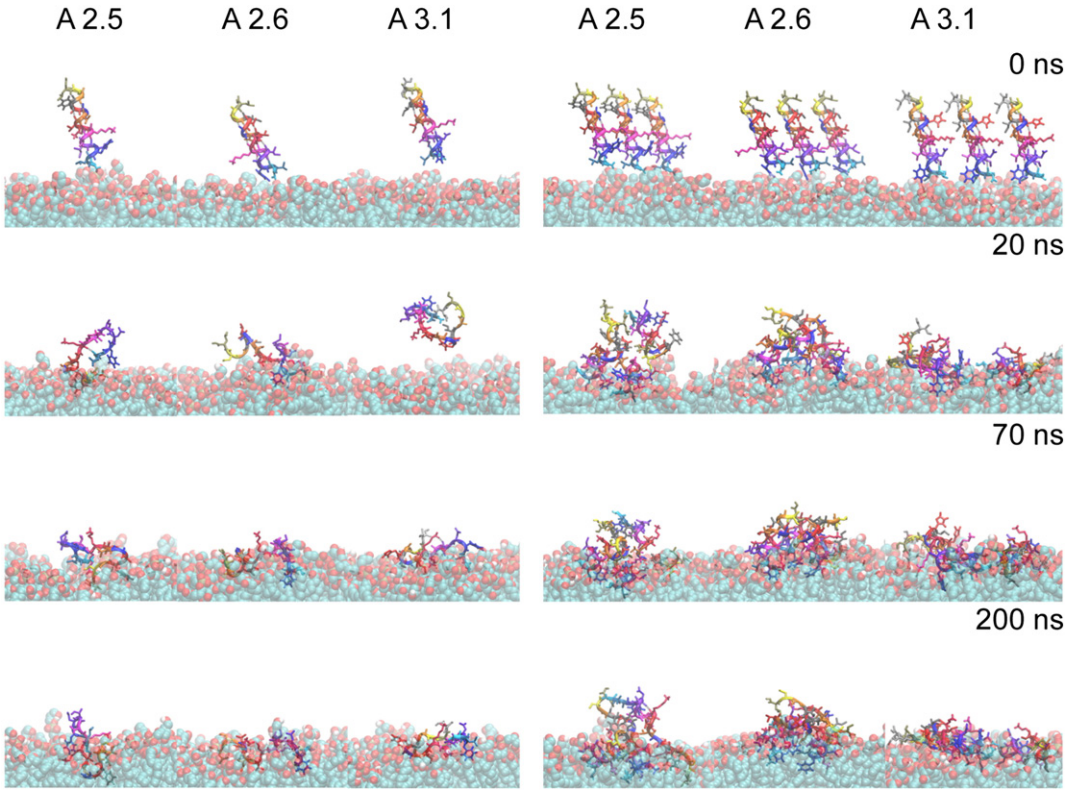

Fig. 7. Simulation snapshots of single and triple aureins with POPG lipid bilayers (times are indicated above the snapshots).

interface where the LEU2, PHE3 and SER15 form hydrogen bonds with the PO_4 groups in the bilayer. After 200 ns, PHE3 inserts deeply into the membrane and residues VAL9, ILE10, ILE13, and LEU16 penetrate into the hydrophobic core region. In contrast to both aurein 2.5-COOH and aurein 2.6-COOH, aurein 3.1-COOH interactsmainly with the phospholipid headgroup region. After 20 ns HIS12 interacts with the headgroup region via electrostatic interactions. After 70 ns the backbone of GLY11 forms a hydrogen bond with the hydroxyl group of the headgroup of POPG and the peptide lies parallel to the membrane surface. After 200 ns the peptide is in contact with the headgroup region of the membrane surface (Fig. 7).

3.2.4. Multiple aureins in POPG

In the presence of POPG a deeper penetration of AMPs occurs. In the case of aurein 2.5-COOH after 20 ns an unstable peptide trimer is formed (Fig. 7). However, after 70 ns peptide–peptide connections are formed between LEU2 of peptide C and PHE13 residue of peptides A and B enabling deeper penetration into the membrane driven by hydrophobic interactions. After 200 ns a hydrophobic core is created involving PHE3, ILE5 and VAL6 residues peptide C and PHE13 residues of peptides A and B while residues PHE13 and LEU16 of peptide C insert into the headgroup region. In the case of aurein 2.6-COOH, the peptides also form a trimer in the presence of POPG involving residues VAL12 and LEU16 of peptide A, LEU2, VAL9, and ILE10 of peptide B, and VAL9, ILE10, and LEU16 of the peptide C. The trimer is stabilized by four intermolecular hydrogen bonds between the three peptides. After 70 ns, the trimer approaches the membrane interface due to electrostatic interaction with POPG headgroup region. The hydrophobic pore is stabilized using residues VAL9 of peptide A, LEU2, LEU5, VAL9, and ILE10 of peptide B and ILE5, VAL9, ILE13, and LEU16 of peptide C. After 200 ns the hydrophobic core is created involving VAL12 of peptide A, LEU2, VAL9, and ILE10 of peptide B, ILE5 and VAL9 of peptide C. The core inserts into the lipid bilayer. In contrast to both aurein 2.5-COOH and aurein 2.6-COOH, in the case of aurein 3.1-COOH there is no pore formation. At the start of the simulation LEU2 and PHE3 orientates and approaches the membrane interface where the hydrophobic residues interact with alkyl chains of POPG lipid bilayer. After 70 ns a dimer is formed between peptides B and C, which facilitates deeper penetration into the lipid bilayer via the side chains of LEU2 of peptide B and PHE3 of peptide C. At 200 ns the dimerisation occurs between peptide B and peptide C involving the side chains of PHE3 and the alkyl group of the side chain of LYS7 of peptide B and residues ILE5, ILE9, and ILE13 of peptide C. The hydrogen bonds are formed between the PHE3 residues of peptides B and C and the PO_4 group of the lipid bilayer. In addition, the GLY1 residue of peptide C and GLY15 residue of peptide B form a hydrogen bond with hydroxyl groups of the headgroups of lipid bilayer (Fig. 7).

3.2.5. Distance between the peptide and the lipid bilayer

Fig. 8 shows distances between the centre of the mass of aurein peptides and the top leaflet P atoms of a lipid bilayer in the case of one and three peptides. The single peptides approach the headgroups of the lipid bilayer faster compared to peptide trimer. In the presence of a POPE bilayer the distance between aurein 2.5-COOH, aurein 3.1-COOH and the lipid bilayer is 1 nm away from the membrane (Fig. 8). However, in the case of the single aurein 2.6-COOH the minimal distance is 1.5 nm. For a POPG bilayer, in the case of a single peptide the distance between bilayer and either the aurein 2.5-COOH and aurein 2.6-COOH is 0.5 nm. In contrast, for aurein 3.1-COOH in a POPG bilayer the minimal distance is 1.5 nm.

In the case of three aurein 2.5-COOH peptides the distances from the P atoms to the top leaflet of the POPE lipid bilayer is 2.5 nm. The interaction with the lipid bilayer is enhanced by the peptide–peptide

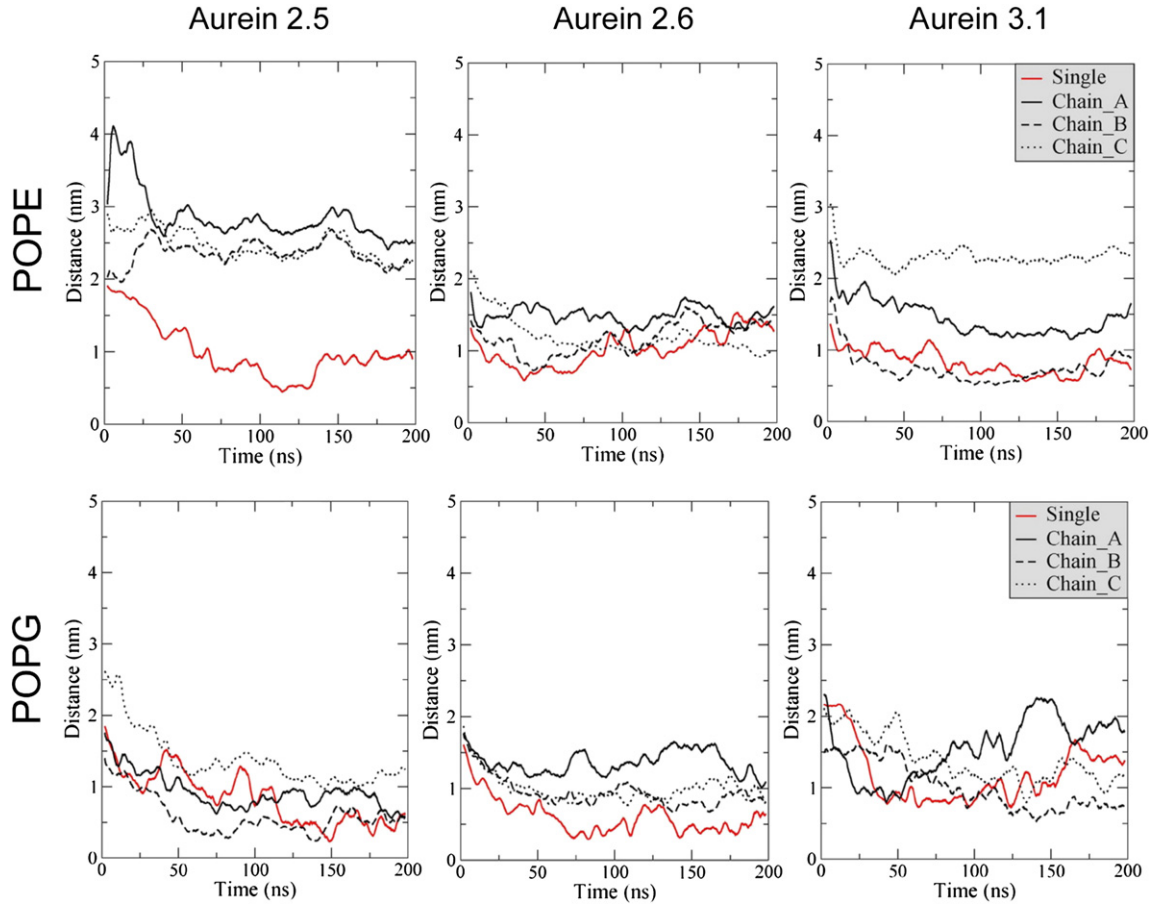

Fig. 8. Distances between the centre of the mass of peptides and the P atoms of the top leaflet of a lipid bilayer.

cooperation and hence the distance between peptide and lipid bilayer is significantly different for the single one and the three peptides (see e.g. Fig. 8 top left). For aurein 2.6-COOH peptides A and B are 1.5 nm away from POPE, while peptide C is inserted deeper into the membrane (about 1 nm away from the membrane). The distance between the aurein 3.1-COOH peptide B and POPE is about 0.8 nm. Peptides A and C are 1.5 nm and 2.3 nm away from POPE, respectively (Fig. 8). In the presence of POPG a different dynamic picture is observed. For three aurein 2.5-COOH, peptides A and B are circa 0.5 nm away from POPG, while the distance between POPG and peptide C is 1 nm. For three aurein 2.6-COOH molecules the distance from POPG bilayer is 1 nm (Fig. 7). In the case of three aurein 3.1-COOH molecules the distance between peptide B and POPG is 0.5 nm (Fig. 8) whereas peptides A and C are 1 nm away from the P atoms of POPG (Fig. 8). Regarding the integrity of the membrane, the area per lipid for single and triple peptides is stable and it is in accordance with the previous computational works (see Figs. S1-S3) [56,51]. Moreover the thickness of lipid bilayer in the presence of peptide shows that in POPE lipid bilayer multiple aureins 2.5-COOH and 2.6-COOH form compact complexes while aurein 3.1-COOH remains separate (see Fig. S2). In POPG all aureins do not form compact complexes but they are spread over large lipid areas (see Fig. S3).

3.3. Cooperative vs non-cooperative behaviour

All the peptides studied here show a cooperative behaviour in the presence of water, while in the presence of TFE no cooperativity is observed. This is confirmed by the hydrogen bond (HB) analysis (see Fig. S4) in the presence of water. The highest number of HBs (aurein-water, inter and intra bond) is observed for the aurein 3.1-COOH. The inter HBs of aureins 2.5-COOH, 2.6-COOH and 3.1-COOH are observed only between two peptides, for example in the case of aurein 2.5-COOH between peptide A and peptide B one HB is observed, while between peptides A and C and between peptides B and C four and seven HBs are observed respectively. It shows a cooperativity leading to the assembly of peptide dimers into a trimer chain structure. Our data demonstrate in the presence of lipid bilayer different collective behaviour of aureins 2.5-COOH and aurein 2.6-COOH compared with aurein 3.1-COOH. Aurein 3.1-COOH shows a lower number of inter-peptide HB compared with aurein 2.5-COOH and 2.6-COOH showing less cooperative behaviour. While aurein 2.5-COOH and aurein 2.6-COOH form trimer prior to insertion into the bilayers, aurein 3.1-COOH does not exhibit such collective behaviour. In the present study we find that the cooperativity between the peptides is driven by the hydrophobic amino acids and accompanied by a difference in the secondary structure and by the interaction of the peptides with the lipid bilayer. For three aurein 2.5-COOH and aurein 2.6-COOH molecules in the presence of either POPE or POPG a similar behaviour was observed. The two peptides formed a trimer, which created a hydrophobic pore involving the polar residues being exposed to the lipid/water interface (Figs. 6 and 7). As the peptides approach a POPG membrane, the hydrophobic channel reduces in size due to the increased interaction between the hydrophobic residues and the lipid bilayer. Hence, the aggregation of the peptides due to the cooperativity occurs in the initial stage of the binding process. In contrast to a POPG membrane aurein 2.5-COOH and aurein 2.6-COOH penetrate at a slower rate into a POPE membrane (Fig. 6) although again a trimer is formed prior to membrane penetration. However, peptides can also accumulate at the membrane interface without cooperativity. Aurein 3.1-COOH interacts with the membrane without a strong cooperativity (only a transient trimer is formed). However, aurein 2.5-COOH and aurein 2.6-COOH exhibit a co-operative effect in the presence of POPE and POPG, which has been shown to be the key to the membrane interaction (Figs. 6 and 7). The difference in the cooperativity behaviour of the aureins studied here can be understood from the hydrophobicity surface map in Fig. 9. As we can see aurein 2.5-COOH and aurein 2.6-COOH have a rather similar charge distribution while aurein 3.1-COOH is distinctly different. The difference in aurein 3.1-COOH is mostly due to a significantly larger area of the negative charge as a result of HIS-residue presence. After 200 ns the hydrophobic surface map is drastically changed due to the attempt to minimize the solvent accessible surface area. In the case of aurein 2.5-COOH and aurein 2.6-COOH the hydrophobic and hydrophilic areas are well localized, while in aurein 3.1-COOH the hydrophilic area is rather spread.

For all the peptides in the presence of a lipid bilayer we observe a partial penetration into the membrane. Both the aurein 2.5-COOH and aurein 2.6-COOH aggregate forming a trimer before interacting with the membrane/water interface. This behaviour is similar to the one reported by Marrink et al. [19,20] where they performed several MD simulations of melittin in DPPC membrane at different concentrations. It was found that these peptides always aggregate into dimer, trimer or tetramer. In these simulations the melittin peptides move towards the membrane interface rapidly (within 5 ns) while in our case the peptides aurein 2.5-COOH and 2.6-COOH bind to the membrane within 20 ns. The aurein 3.1-COOH in POPG needs even more than 20 ns to arrive to the interface. After 200 ns of simulation our peptides just start to form a pore in the membrane (see Fig. 7). It is evident from Fig. 8 that the higher peptides/lipid concentration results in a deeper penetration in agreement with the results in Refs. [19,20]. However the aurein 3.1-COOH behaves differently compared to aureins 2.5-COOH and 2.6-COOH. At higher concentrations aurein 3.1-COOH behaves as a single peptide only occasionally forming an unstable dimer.

3.4. Conclusions

In summary, molecular dynamics simulation of aureins 2.5-COOH, 2.6-COOH and 3.1-COOH in water, TFE, POPE and POPG have been performed to investigate the cooperative effect on their antimicrobial activity. The MD simulations were accompanied by CD measurements. The

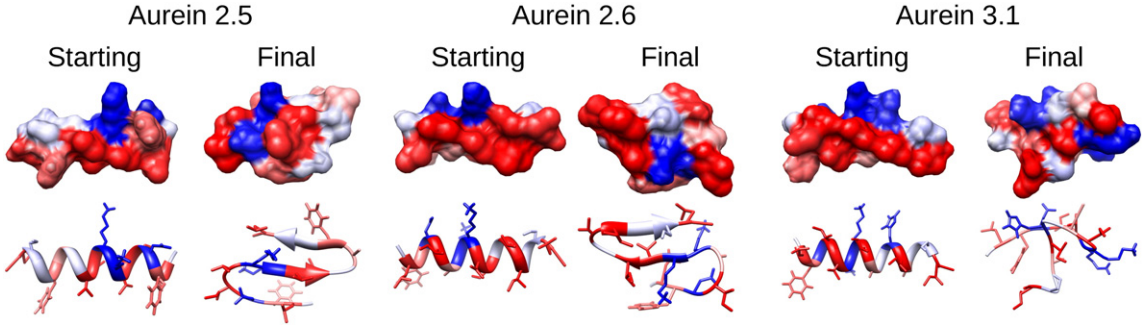

Fig. 9. Hydrophobicity surfaces of aurein 2.5-COOH, 2.6-COOH and aurein 3.1-COOH for the initial and final configurations in water environment. Red denotes the excess of positive charge, blue - the excess of negative charge and white is neutral.

results show that the studied peptides have stronger intermolecular interactions in aqueous solution than in TFE. The α-helix structure is preserved in TFE while in water the peptides unfold into a β-sheet secondary structure. In the presence of a lipid bilayer single and multiple aurein molecules behave differently. In the case of a single peptide a stable secondary structure is observed in POPE, while for three aureins a greater stability of the α-helix has been observed for POPG. In POPE and POPG the aureins 2.5-COOH and 2.6-COOH form a hydrophobic aggregate to minimize the interaction between the hydrophobic groups and the water. Once it reaches the water/lipid interface the peptide aggregate starts collectively to penetrate into the membrane. In contrast, aurein 3.1-COOH forms a transient hydrophobic aggregate and once it reaches the water/lipid interface it disintegrates and the aureins behave as the single ones.

4. Associated content

Characterisation of lipid bilayer stability is shown in Figs. S1–S3. Fig. S4 shows the inter-molecular HBs of the three peptides in water.

Acknowledgement

MM thanks the Volkswagen Foundation (Germany) for the financial support (Ref.: 83932). All simulations were carried out at the UCLan High Performance Computing Facilities.

Appendix A. Supplementary data

Supplementary data to this article can be found online at http://dx.doi.org/10.1016/j.bbamem.2014.07.002.

References

[1] Y. Li, Q. Xiang, Q. Zhang, Y. Huang, Z. Su, Overview on the recent study of antimicrobial peptides: origins, functions, relative mechanisms and application, Peptides 37 (2012) 207–215.
[2] L. Brandenburg, J. Merres, L.-J. Albrecht, D. Varoga, T. Pufe, Antimicrobial peptides: multifunctional drugs for different applications, Polymer 4 (2012) 539–560.
[3] M. Zasloff, Antimicrobial peptides of multicellular organisms, Nature 415 (2) (2002) 389–395.
[4] E.F. Palermo, S. Vemparala, K. Kuroda, Cationic spacer arm design strategy for control of antimicrobial activity and conformation of amphiphilic methacrylate random copolymers, Biomacromolecules 13 (5) (2012) 1632–1641.
[5] J.L. Fox, Antimicrobial peptides stage a comeback, Nat. Biotechnol. 31 (2013) 379–382.
[6] D.A. Phoenix, S.R. Dennison, F. Harris, Antimicrobial Peptides, Wiley, London, 2013.
[7] W.C. Wimley, K. Hristova, Antimicrobial peptides: successes, challenges and unanswered question, J. Membr. Biol. 239 (2011) 27–34.
[8] D.E. Schlamadinger, Y. Wang, J.A. McCammon, J.E. Kim, Spectroscopic and Computational Study of Melittin, Cecropin A, and the Hybrid Peptide CM15, J. Phys. Chem. B 116 (35) (2012) 10600–10608.
[9] H. Sato, J.B. Feix, Peptide–membrane interactions and mechanisms of membrane destruction by amphipathic Î ± -helical antimicrobial peptides, Biochim. Biophys. Acta (2006) 1245–1256.
[10] D.W. Hoskin, A. Ramamoorthy, Studies on anticancer activities of antimicrobial peptides, Biochim. Biophys. Acta (2008) 357–375.
[11] D.I. Fernandez, A.P. Le Brun, T. Whitwell, M.-A. Sani, M. James, F. Separovic, The antimicrobial peptide aurein 1.2 disrupts model membranes via the carpet mechanism, Phys. Chem. Chem. Phys. 14 (2012) 15739–15751.
[12] C. Kim, J. Spano, E.-K. Park, S. Wi, Evidence of pores and thinned lipid bilayers induced in orientated lipid membranes interacting with the antimicrobial peptides, magainin-2 and aurein-3.3, Biochim. Biophys. Acta 1788 (2009) 1482–1496.
[13] P. Wadhwani, E. Strandberg, N. Heidenreich, J. Bürck, S. Fanghänel, A.S. Ulrich, Self-assembly of flexible β-strands into immobile amyloid-like β-sheets in membranes as revealed by solid-state 19F NMR, J. Am. Chem. Soc. 134 (15) (2012) 6512–6515.
[14] N. Lu, K. Yang, B. Yuan, Y. Ma, Molecular response and cooperative behavior during the interactions of melittin with a membrane: dissipative quartz crystal microbalance experiments and simulations, J. Phys. Chem. B 116 (31) (2012) 9432–9438.
[15] C. Chen, F. Pan, S. Zhang, J. Hu, M. Cao, J. Wang, H. Xu, X. Zhao, J.R. Lu, Antibacterial activities of short designer peptides: a link between propensity for nanostructuring and capacity for membrane destabilization, Biomacromolecules 11 (2) (2010) 402–411.
[16] K. Bertelsen, J. Dorosz, S.K. Hansen, N.C. Nielsen, T. Vosegaard, Mechanisms of peptide-induced pore formation in lipid bilayers investigated by oriented P-31 solid-state NMR spectroscopy, PLoS ONE 7 (10) (2012) e47745.
[17] L. Chen, N. Patrone, J.F. Liang, Peptide self-assembly on cell membranes to induce cell lysis, Biomacromolecules 13 (10) (2012) 3327–3333.
[18] Y. He, L. Prieto, T. Lazaridis, Modeling peptide binding to anionic membrane pores, J. Comput. Chem. 34 (2013) 1463–1675.
[19] D. Sengupta, H. Leontiadou, A.E. Mark, S.J. Marrink, Toroidal pores formed by antimicrobial peptides show significant disorder, Biochim. Biophys. Acta 1778 (2008) 2308–2317.
[20] H. Leontiadou, A.E. Mark, S.J. Marrink, Antimicrobial peptides in action, J. Am. Chem. Soc. 128 (2006) 12156–12161.
[21] Y. Li, H. Guo, Atomistic simulations of an antimicrobial molecule interacting with a model bacterial membrane, Theor. Chem. Accounts 132 (2013) 1303.
[22] Y. Wang, D.E. Schlamadinger, J.E. Kim, J.A. McCammon, Comparative molecular dynamics simulations of the antimicrobial peptide CM15 in model lipid bilayers, Biochim. Biophys. Acta 1818 (5) (2012) 1402–1409.
[23] H. Tao, S.C. Lee, A. Moeller, R.S. Roy, F. Siu, J. Zimmermann, R.C. Stevens, C.S. Potter, B. Carragher, Q. Zhang, Engineered nanostructured β-sheet peptides protect membrane proteins, Nat. Methods 10 (2013) 759–761.
[24] K. Witte, B.E.S. Olausson, A. Walrant, I.D. Alves, A. Vogel, Structure and dynamics of the two amphipathic arginine-rich peptides rw9 and rl9 in a lipid environment investigated by solid-state nmr and md simulations, Biochim. Biophys. Acta 1828 (2013) 824–833.
[25] G. Kokot, M. Mally, S. Svetina, The dynamics of melittin-induced membrane permeability, Eur. Biophys. J. 41 (2012) 461–474.
[26] M. Pourmousa, M. Karttunen, Early stages of interaction of cell-penetrating peptide penetrating with dppc bilayer, Chem. Phys. Lipids 169 (2013) 85–94.
[27] M. Pourmousa, J. Wong-ekkabut, M. Patra, M. Karttunen, Molecular dynamics studies of trasportan interacting with a dppc lipid bilayer, J. Phys. Chem. B 117 (2013) 230–241.
[28] P.J. Bond, S. Khalid, Antimicrobial and cell-penetrating peptides: structure, assembly and mechanisms of membrane lysis via atomistic and coarse-grained molecular dynamic simulations, Protein Pept. Lett. 17 (11) (2010) 1313–1327.
[29] M. Mihajlovic, T. Lazaridis, Charge distribution and imperfect amphipathicity affect pore formation by antimicrobial peptides, Biochim. Biophys. Acta 1818 (2012) 1274–1283.
[30] A.J. Krauson, J. He, W.C. Wimley, Determining the mechanism of membrane permeabilizing peptides: indentification of potent, equilibrium pore-formers, Biochim. Biophys. Acta 1818 (2012) 1625–1632.
[31] B.S. Perrin, Y. Tian, R. Fu, C.V. Grant, E.Y. Chekmenev, W.E. Wieczorek, A.E. Dao, R.M. Hayden, C.M. Burzynski, R.M. Venable, M. Sharma, S.J. Opella, R.W. Pastor, M.L. Cotten, High-resolution structures and orientations of antimicrobial peptides piscidin 1 and piscidin 3 in fluid bilayers reveal tilting, kinking, and bilayer immersion, J. Am. Chem. Soc. 136 (2014) 3491–3504.
[32] T.G. Castro, N.M. Micaêlo, Modeling of peptaibol analogues incorporating nonpolar α, α-dialkyl glycines shows improved α-helical preorganization and spontaneous membrane permeation, J. Phys. Chem. B 118 (2014) 649–658.
[33] P.J. Bond, M.S.P. Sansom, Insertion and assembly of membrane proteins via simulations, J. Am. Chem. Soc. 128 (2006) 2697–2704.
[34] D.L. Parton, E.V. Akhmatskaya, M.S.P. Sansom, Multiscale simulations of the antimicrobial peptide maculatin 1.1: water permeation through disordered aggregates, J. Phys. Chem. B 116 (29) (2012) 8485–8493.
[35] K.P. Santo, S.J. Irudayam, M.L. Berkowitz, Melittin creates transient pores in a lipid bilayer: results from computer simulations, J. Phys. Chem. B 117 (2013) 5031–5042.
[36] W. Shinoda, R. De Vane, M.L. Klein, Computer simulation studies of self-assembrly macromolecules, Curr. Opin. Struct. Biol. 22 (2012) 175–186.
[37] P.J. Bond, D.L. Parton, J.F. Clark, M.S.P. Sansom, Coarse-grained simulations of the membrane-active antimicrobial peptide maculatin 1.1, Biophys. J. 95 (8) (2008) 3802–3815.
[38] R. Chen, A.E. Mark, The effect of membrane curvature on the conformation of antimicrobial peptides: implication for binding and the mechanism of action, Eur. Biophys. J. 40 (2011) 545–553.
[39] S.J. Irudayam, M.L. Berkowitz, Binding and reorientation of melittin in a popc bilayer: computer simulations, Biochim. Biophys. Acta 1818 (2012) 2975–2981.
[40] M. Mura, S.R. Dennison, A.V. Zvelindovsky, D.A. Phoenix, Aurein 2.3 functionality is supported by oblique orientated α-helical formation, Biochim. Biophys. Acta Biomembr. 1828 (2) (2013) 586–594.
[41] A.A. Polyansky, A.O. Chugunov, A.A. Vassilevski, E.V. Grishin, R.G. Efremov, Recent advances in computational modeling of helical membrane-active peptides, Curr. Protein Pept. Sci. 13 (2012) 644–657.
[42] A.J. Mason, P. Bertani, G. Moulay, A. Marquette, B. Perrone, A.F. Drake, A. Kichler, B. Bechinger, Membrane interaction of chrysophsin-1, a histidine-rich antimicrobial peptide from red sea breamâ€, Biochemistry 46 (2007) 15175–15187.
[43] J. Cheng, J. Hale, M. Elliott, R. Hancock, S. Straus, The importance of bacterial membrane composition in the structure and function of aurein 2.2 and selected variants, Biochim. Biophys. Acta 1808 (2011) 622–633.
[44] L. Whitmore, B.A. Wallace, Dichroweb, an online server for protein secondary structure analyses from circular dichroism spectroscopic data, Nucleic Acids Res. 32 (2004) W668–W673.
[45] L. Whitmore, B.A. Wallace, Protein secondary structure analyses from circular dichroism spectroscopy: methods and reference databases, Biopolymers 89 (2008) 392–400.
[46] L. Whitmore, B. Woollett, A.J. Miles, R.W. Janes, B.A. Wallace, The protein circular dichroism data bank, a web-based site for access to circular dichroism spectroscopic data, Structure 18 (2010) 1267–1269.
[47] D. Van Der Spoel, E. Lindahl, B. Hess, G. Groenhof, A.E. Mark, H.J.C. Berendsen, GROMACS: fast, flexible, and free, J. Comput. Chem. 26 (16) (2005) 1701–1718.

[48] B. Hess, C. Kutzner, D. van der Spoel, E. Lindahl, GROMACS 4: algorithms for highly efficient, load-balanced, and scalable molecular simulation, J. Chem. Theory Comput. 4 (3) (2008) 435–447.
[49] D. van der Spoel, P.J. van Maaren, H.J.C. Berendsen, A systematic study of water models for molecular simulation: derivation of water models optimized for use with a reaction field, J. Chem. Phys. 108 (1998) 10220–10230.
[50] T.J. Piggot, D.A. Holdbrook, S. Khalid, Electroporation of the *E. coli* and *S. aureus* membranes: molecular dynamics simulations of complex bacterial membranes, J. Phys. Chem. B 115 (45) (2011) 13381–13388.
[51] A. Kukol, Lipid models for united-atom molecular dynamics simulations of proteins, J. Chem. Theory Comput. 5 (3) (2009) 615–626.
[52] D.P. Tieleman, Computational methods to model membrane dynamics, Membrane Dynamics, vol. 5, Academic Press, University of Virginia, VA, USA, 2012.
[53] B. Hess, H. Bekker, H.J.C. Berendsen, J.G.E.M. Fraaije, Lincs: a linear constraint solver for molecular simulations, J. Comput. Chem. 18 (1997) 1463–1472.
[54] R.P. Joosten, T.A.H. te Beek, E. Krieger, M.L. Hekkelman, R.W.W. Hooft, R. Schneider, C. Sander, G. Vriend, A series of pdb related databases for everyday needs, Nucleic Acids Res. (2010) 1–9.
[55] W. Kabsch, C. Sander, Dictionary of protein secondary structure: pattern recognition of hydrogen-bonded and geometrical features, Biopolymers 22 (1983) 2577–2637.
[56] D.P. Tieleman, L.R. Forrest, M.S.P. Sansom, H.J.C. Berendsen, Lipid properties and the orientation of aromatic residues in ompf, influenza m2 and alamethicin systems: molecular dynamics simulations, Biochemistry 37 (1998) 17554–17561.